

# Modeling and Experimental Investigation of Material Microstructure Effects on Cutting Force and Surface Roughness during Micro Endmilling on Inconel 718

Anand Krishnan N<sup>1</sup>, Ankit Awasti<sup>2</sup> and Jose Mathew<sup>3</sup>

<sup>1,2,3</sup> Department of Mechanical Engineering, National Institute of Technology Calicut, Kerala - 673601, INDIA

## Abstract

Micro milling is one of the most preferred micro machining process because of its flexibility and ability to produce complex three dimensional micro components. Accurate prediction of cutting force during micro endmilling is significant in characterizing the cutting process, as it plays an important role in the surface quality and tool wear. This paper presents a mathematical model to predict the cutting force during micro endmilling process under various cutting conditions by considering the material microstructure and cutting edge radius effect. Experiments were performed on Inconel 718, an aerospace alloy, to validate the model. Cutting force and areal surface roughness were taken as responses to understand their variations with feed per tooth. Cutting force was measured by using KISTLER mini dynamometer (9256C2), areal surface roughness was measured by using 3D optical profiler (Infinite focus G5, Alicona). Developed force model was validated with the experimental results and identified that the material microstructure significantly affects the flow stress and thereby the cutting force. It was observed that for feed per tooth less than the size effect zone, cutting force shows a nonlinear trend. The minimum areal surface roughness ( $S_a$ ) was found to be in the range of  $3\mu\text{m}$ , which is the cutting edge radius of the tool.

Keywords: Micro endmilling, material microstructure, cutting force model, Inconel 718, areal surface roughness

## 1. INTRODUCTION

Over last decade, increasing demand on micro parts and products has led to high requirements on high quality micro fabrication processes. Micro sized product is a growing area of interest for industry as well as for research community because of its wide spread applications. Micro parts and products are being widely used in many areas such as optics, electronics, biomedical devices, communication, avionics, etc. Micro end milling is one of the preferred manufacturing method to produce micro parts because of its flexibility and ability to produce complex 3D parts. In micro endmilling the cutter diameter will be upto  $500\mu\text{m}$ . One of the main challenges in micro machining is to produce parts with good surface quality. Poor surface finish will affect proper fitting, dimensional accuracy and assembly of the parts. In micro cutting chip is generated only when the unformed chip thickness greater than a critical value, called minimum uncut chip thickness (MUCT). As we downscale from macro to micro machining, so many factors become prominent which should be considered in machining analysis. In micro machining, the interaction between tool and workpiece is of crystal level so crystallographic impurities plays an important role in micro machining analysis. The machining force and surface finish are greatly affected by micro structural orientation due to high influence of grain boundaries, micro-cracks and voids in micro machining. That's why, it is very important to analyse the microstructure effects in machining for investigating the flow stress, cutting force and surface integrity.

Researches have been done to analyse the behavior of Inconel 718 under different machining conditions. Iturbe et al. [1] have done the analysis to assess the machinability of Inconel 718 by micro hardness measurement and microstructural analysis of samples at high temperature and strain rate. The correlation is also developed for relating mechanical properties of Inconel 718 with microstructural state.

The effect of microstructure on flow stress and cutting force on Inconel 718 is also analysed for conventional milling process. The analysis is done considering the effect of grain growth and

dynamic recrystallization due to high temperature generated during machining. The grain growth improves machinability due to reduced flow stress. Softening effect such as preheating is also used to reduce the cutting force. The grain size dependent cutting force models are developed to consider the recrystallization effect [2-3]. The effect of grain boundaries, grain size and crystallographic orientation on flow stress and cutting forces is also analysed [4]. Rahman et al. [5] also investigated the effect of chip thickness and grain size on flow stress. The variation of surface quality and micro-chip morphology due to varying tool sharpness and grain size is also analysed.

Majority of works related to microstructure are based on the experimental investigation. Pan et al. [6] developed the model having the thermal, mechanical and microstructural coupled analysis during machining. The analysis is also considered the microstructural changes occurred in work piece during machining. The changes in surface integrity and mechanical properties due to microstructure change are also investigated. Vogler et al. [7] developed the algorithm for considering the effect of minimum uncut chip thickness. The slip-line plasticity model for finding force is used when uncut chip thickness is more than the minimum chip thickness and elastic deformable model for force is used when uncut chip thickness is less than the minimum chip thickness. Simulation is done at microstructure level for finding the parameters of force model.

This paper presents an attempt to model material microstructure effects on cutting forces during micro end milling of Inconel 718. Experimental results are verified with the proposed model. Finally a detailed analysis of the cutting force and areal surface roughness ( $S_a$ ) were carried out for a wide range of feed per tooth and overall conclusions were reported.

## 2. MODELING OF CUTTING FORCE

Cutting force was modeled based on the flow stress model which considered the grain size, grain boundaries and crystallographic orientation were shown in Equation (1) [4].

\*Correspondence author Email: anandkrish487@gmail.com

$$\sigma = \bar{\sigma}_{JC}(\varepsilon, \dot{\varepsilon}, T) + M\alpha_b G b \sqrt{\frac{k\theta_{av}}{D_{avg}b}} + K_{HP}(\varepsilon, \dot{\varepsilon}, T) D^{-\frac{1}{2}} \quad (1)$$

Where  $\bar{\sigma}_{JC}$  is the flow stress as a function of strain, strain rate, and temperature can be obtained from Johnson-Cook model as in Equ. 2.  $K_{HP}$  is the Hall-Petch coefficient,  $D$  is the grain size,  $M$  is the Taylor factor,  $D_{avg}$  is the average grain size taken as  $D$  here.  $\theta_{avg}$  is the average misorientation angle,  $G$  is the shear modulus,  $k$  and  $\alpha_b$  are materials constants.

$$\bar{\sigma}_{JC} = [A + B(\varepsilon)^n]_x \left[ 1 + C \ln \left( \frac{\dot{\varepsilon}}{\dot{\varepsilon}_0} \right) \right]_x \left[ 1 - \left( \frac{T - T_0}{T_m - T_0} \right) \right] \quad (2)$$

Where  $\varepsilon$  is the equivalent plastic strain,  $\dot{\varepsilon}$  is the equivalent plastic strain rate, and  $\dot{\varepsilon}_0$  is the reference plastic strain rate, always  $\dot{\varepsilon}_0 = 1.0/s$ ,  $T$  is the cutting temperature,  $T_m$  melting temperature and  $T_0$  is room temperature.  $n$  and  $m$  are the strain hardening index and thermal softening index respectively.  $A$ ,  $B$  and  $C$  are J-C Parameters represent the yield strength, strain and strain rate sensitivities of the material. Table 1 shows the J-C parameters for Inconel 718 [8].

**Table 1**

Johnson-Cook constitutive model parameters for Inconel 718

A (MPa)	B (MPa)	C	n	m
450	1700	0.017	0.65	1.3

$$K_{HP} = M \sqrt{\frac{\tau_b 4Gb}{(1-\nu)\pi}} \quad (3)$$

Where  $M$  is the Taylor factor,  $G$  is the shear modulus,  $\nu$  is the poisson ratio.  $\tau_b$  is the critical grain boundary stress obtained from Equation(4)[10].

$$\tau_b = 0.057G \quad (4)$$

The value of flow stress,  $\sigma$  can then be utilized to determine the shear plane force and plane normal force by substituting it in Equation(7) and (8). The possibility of elastic recovery of the workpiece material is very important in micromachining. The tool work piece contact length,  $L_f$  can be obtained as in Equation (6) [9]

$$L_f = \frac{S}{\sin \theta_f} \quad (5)$$

Where,  $S$  is spring back which is equal to  $k_1 r_e H/E$ ,  $k_1$  is a constant,  $r_e$  tool cutting edge radius,  $H$  Vicker's hardness,  $E$  material elastic modulus and  $\theta_f$  is relief angle of tool. When only shear plane shear occur shear plane force ( $F_s$ ) and shear plane normal force ( $N_s$ ) can be expressed as [9]

$$F_s = \frac{(\sigma/\sqrt{3}) b d}{\sin \phi} \quad (6)$$

$$N_s = \frac{\sigma b d}{\sin \phi} \quad (7)$$

Where,  $b$  is width of cut,  $d$  is depth of cut in orthogonal cutting,  $\phi$  shear angle and  $\sigma$  is flow stress of the workpiece material. In order to consider spring back effect of workpiece material during micro machining an additional frictional force owing to increase in work piece tool contact length has been included in the force model proposed by [9] as flank face contact force ( $F_{fc}$ ) and flank face normal force ( $F_{fn}$ ). This can be obtained as given in the Equation(8) and Equation(9).

$$F_{fc} = \frac{CY}{\sqrt{3}} L_f b \quad (8)$$

$$F_{fn} = CY L_f b \quad (9)$$

By adding above friction force components, new principal cutting force and thrust cutting force obtained from Merchant's circle diagram as in Equation(10) and Equation (11).

$$F_c = F_s \cos \phi + N_s \sin \phi + F_{fc} \quad (10)$$

$$F_t = -F_s \sin \phi + N_s \cos \phi + F_{fn} \quad (11)$$

For micro end milling process chip thickness varies with tool rotation angle, so we can write chip thickness ( $t$ ) as a function of tool rotation angle as given in the Equation(12).

$$t = f_t \sin \theta \quad (12)$$

Where,  $f_t$  is feed per tooth and  $\theta$  is tool rotation angle. By incorporating this  $t$  in Equation (6) and (7) and using Equation(8) and(9), we can get final expression for principal cutting force and thrust force. An expression for  $F_X$  and  $F_Y$  was derived [9] as given below:

$$F_X = [C_1(\sin^2 \theta_e - \sin^2 \theta_s) + C_2(\sin 2\theta_e - \sin 2\theta_s) + C_4(\sin \theta_e - \sin \theta_s) + C_5(\cos \theta_e - \cos \theta_s) + C_3(\theta_e - \theta_s)] \quad (13)$$

$$F_Y = [C_3(\sin^2 \theta_e - \sin^2 \theta_s) + 0.5C_1(\sin 2\theta_e - \sin 2\theta_s) - C_5(\sin \theta_e - \sin \theta_s) - C_4(\cos \theta_e - \cos \theta_s) - C_1(\theta_e - \theta_s)] \quad (14)$$

$$\text{Where } C_1 = -\frac{\sigma f_t r \cos \phi}{2\sqrt{3} \sin \phi \tan \psi} - \frac{\sigma f_t r}{2 \tan \psi}$$

$$C_2 = -\frac{\sigma f_t r}{4\sqrt{3} \tan \psi} + \frac{\sigma f_t r \cos \phi}{4 \sin \phi \tan \psi}$$

$$C_3 = \frac{\sigma f_t r}{2\sqrt{3} \tan \psi} - \frac{\sigma f_t r \cos \phi}{2 \sin \phi \tan \psi}$$

$$C_4 = \frac{Y L_f r}{\sqrt{3} \tan \psi}, \quad C_5 = \sqrt{3} C_4$$

$\theta_s$  is the tool start angle and  $\theta_e$  is the tool end angle  $\psi$  and  $\phi$  are the helix angle of the tool and shear angle respectively. Shear angle,  $\phi$ , can be obtained from Merchant's equation (15).

$$\phi = \frac{\pi}{4} + \frac{\alpha}{2} - \frac{\lambda}{2} \quad (15)$$

Where friction angle,  $\lambda$ , was obtained from the coefficient of friction,  $\mu$  which is calculated from experimental force data.  $\alpha$  is the rake angle of the tool. During micromachining process cutting edge radius plays an important role in effective rake angle calculation as shown in Equation(16)

$$\alpha_{eff} = \sin^{-1} \left( \frac{t_0}{r_e} - 1 \right) \text{ For } t_0 < r_e \quad (16)$$

$$\alpha_{eff} = \alpha \text{ For } t_0 > r_e$$

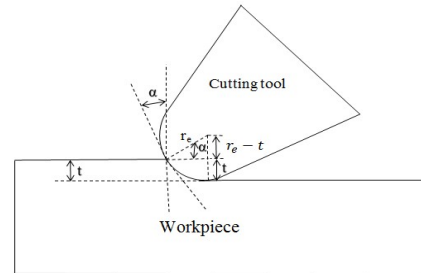


Fig.1 Effective rake angle calculation

### 3. EXPERIMENTAL WORK

#### 3.1 Work piece material

Inconel 718 is used as the workpiece material for this work because of its superior properties like high hardness, high strength to weight ratio, resistance to high temperature loading and resistance to corrosion. Inconel 718 is having wide applications in chemical, nuclear and automobile industries because of its superior mechanical and chemical properties at high temperatures. Table 1 shows the physical properties of Inconel 718 material. The average grain size of the Inconel 718 sheet was in the range of  $6\mu\text{m}$ . Fig. 2 shows the Optical and SEM image of microstructure of Inconel 718. The Grain size was measured by linear intercept method.

Table 1

Properties of Inconel718

Mechanical Properties	Inconel 718
Young's modulus, E	210 GPa
Vickers hardness, H	350
Yield strength, Y	915 MPa
Burgers vector, b	0.254 nm
Taylor factor, M	3.08
Shear modulus, G	75.2 GPa
Poisson ratio ( $\nu$ )	0.3

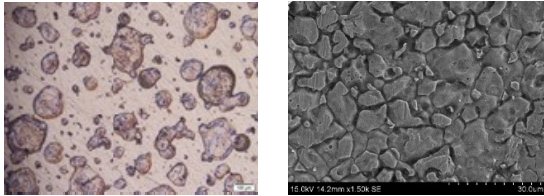


Fig.2. Microstructure of Inconel 718

#### 3.2. Cutting tool

AlTiNcoated WC endmill with  $500\mu\text{m}$  cutter diameter,  $8^\circ$  rake angle and  $10^\circ$  clearance angles were used for this study. Since cutting edge radius has a significant influence on size effect in micromachining, it has been measured physically using optical microscope. Edge radius was measured in the range of  $3\mu\text{m}$ .

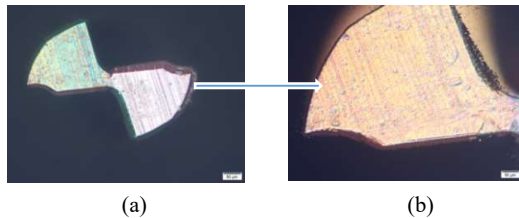


Fig.3. Optical images of (a) Micro end mill cutter and (b) cutter edge radius

#### 3.3. Experimental set up

Experiments were conducted by using micro machining centre (DT110, Mikrottools, Singapore) with AlTiN coated WC micro endmill cutter with a diameter of  $500\mu\text{m}$ . Micro channels of 10 mm length were machined on Inconel 718 work piece. KISTLER dynamometer (9256C2) was used to measure cutting force. Inconel 718 sheet was mounted directly on to the dynamometer.

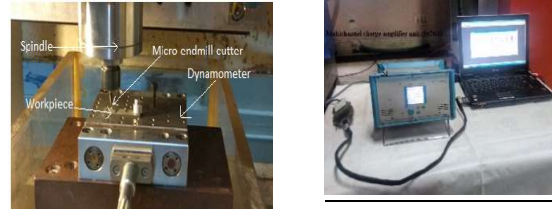


Fig.4. Experimental setup

The configuration of experimental set up for measuring cutting force during micro machining process is shown in the Fig. 4. Areal surface roughness was measured by using 3D optical profiler (Alicona Infinite focus G5) shown in Fig 7.

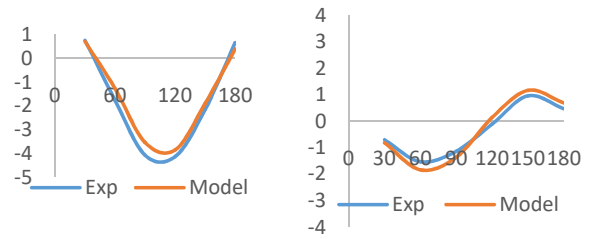
Table 2

Experimental plan

Machine tool	Micro machining centre (DT110, Mikrottools, Singapore)
Cutting speed (m/min)	7.85
Depth of cut (mm)	0.1
Feed per tooth ( $\mu\text{m}$ )	0.1, 0.3, 0.5, 0.7, 0.9, 1.1, 1.3, 1.5, 2, 2.5, 3, 3.5, 4, 4.5, 5, 5.5, 6
Cutting tool	AlTiN Coated WC end mill cutter with $500\mu\text{m}$ diameter
Workpiece material	Inconel718
Dynamometer	KISTLER 9256C2
3D Optical profiler	Alicona Infinite Focus G5

## 4. RESULTS AND DISCUSSION

### 4.1 Cutting force



(a)  $F_x$  for feed/ tooth= $0.5\mu\text{m}$  (a)  $F_y$  for feed/ tooth= $0.5\mu\text{m}$

Fig.5. Experimental and Predicted micro endmilling forces for cutting speed of  $7.85\text{m/min}$  and  $0.1\text{mm}$  depth of cut

Fig. 5 shows the variation of  $F_x$  with rotation angle for both model and experimental data. It can be found that the force trend predicted by the model shows a good agreement with the experimental results. The predicted value of force is near to the experimental results. Deviation from the experimental result may be due to the fact that tool deflection and tool wear were not taken into account in this study.

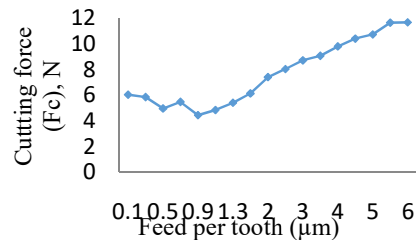


Fig.6. Variation of cutting force Vs feed per tooth for cutting speed of  $7.85\text{m/min}$  and  $0.1\text{mm}$  depth of cut

Fig. 6 shows the variation of cutting force for a wide number of feed per tooth, which is selected by giving equal importance to both size effect and outside size effect region. From the Fig.6 it is clear that above  $1\mu\text{m}$  feed per tooth cutting force increases almost linearly with feed per tooth and below  $1\mu\text{m}$  feed per tooth cutting force deviates from the linear trend. Reason for this could be due to the fact that  $1\mu\text{m}$  falls in the range of minimum uncut chip thickness(MUCT) for the tool used in this study (cutting edge radius of the tool was approximately  $3\mu\text{m}$ ). MUCT is to be in the range of  $1/4$  to  $1/3$  of cutting edge radius [11]. When feed per tooth becomes less than MUCT ploughing is dominated. This is the reason for the increase in cutting force value at lower feed per tooth

#### 4.2 Areal surface roughness

Surface roughness was quantified in terms of areal surface parameter,  $S_a$  and measured using Alicona infinite focus G5.

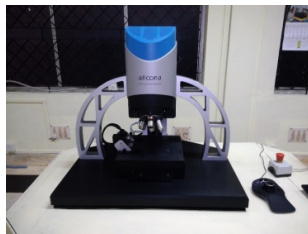


Fig.7 Alicona infinite focus G5

Fig. 8 shows the variation of areal surface roughness for a wide range of feed per tooth. From the Fig. 8 it can be observed that initially as feed per tooth increases areal surface roughness decreases and reaches a minimum value and then increases as feed per tooth increases. This is mainly due to the fact that ploughing is dominant in the region where feed per tooth lesser than cutting edge radius and shearing is dominant in the region where feed per tooth higher than cutting edge radius like in conventional machining. Near to  $3\mu\text{m}$ , which is the cutting edge radius of tool, minimum areal surface roughness were obtained. Similar surface roughness trend was observed in Aramcharoen and Mativenga [12]

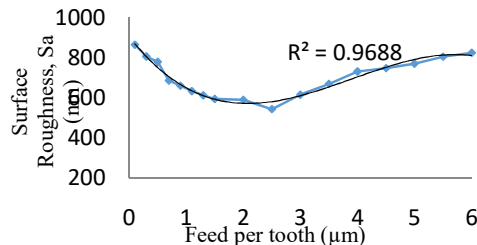


Fig.8. Variation of areal surface roughness ( $S_a$ ) with feed per tooth for cutting speed of  $7.85\text{m/min}$  and  $0.1\text{mm}$  depth of cut

#### 5. CONCLUSIONS

In this paper an attempt have made to modify the micro endmilling cutting force model developed by Kang et al.[9] by incorporating material microstructure and size effect. The cutting force model was successfully validated with experimental results on Inconel 718. Size effect in both cutting force and areal surface roughness were identified. From the Fig.6 it is very clear that near to  $1\mu\text{m}$  feed per tooth, minimum chip thickness is observed, which is in the range of  $1/4^{\text{th}}$  to  $1/3^{\text{rd}}$  of cutting edge radius of the tool [11]. Also found that while machining within the size effect region, areal surface roughness decreases with feed/tooth. Whereas above size effect region

areal surface roughness increases with feed/tooth as in the case of conventional machining.

#### ACKNOWLEDGMENT

Authors would like to sincerely thanks Department of Science & Technology(DST), Govt. of India & Centre for precision measurements & Nanomechanical Testing, Department of Mechanical Engineering, National Institute of Technology Calicut, for providing support to carry out this work under the scheme 'Fund for improvement of Science & Technology' (No. SR/FST/ETI-388/2015).

#### References

- [1] Iturbe A., Giraud E., Hormaetxe E., Garay A., Germain G., Ostolaza K., Arrazola P.J., "Mechanical Characterization and Modelling of Inconel 718 Material Behavior for Machining Process Assessment," *Materials Science & Engineering A*, **682**(2017) 441–453.
- [2] Pan Z., Feng Y., Lu Y.T., Lin Y.F., Hung T.P., Hsu F.C., Lin C.F., Lu Y., Liang S.Y., "Microstructure Sensitive Flow Stress Modeling for Force Prediction in Laser Assisted Milling of Inconel 718," *Manufacturing Review*, **4**(2017)1-9.
- [3] Pan Z., Feng Y., Lu Y.T., Lin Y.F., Hung T.P., Hsu F.C., Liang S., "Force Modeling of Inconel 718 Laser Assisted Endmilling under Recrystallization Effects," *International Journal of Advance Manufacturing Technology*, **92**(2017) 2965–2974.
- [4] Venkatachalam S., Fergani O., Li X., Yang J.G., Chiang K.N., Liang S.Y., "Microstructure Effects on Cutting Forces and Flow Stress in Ultra-Precision Machining of Polycrystalline Brittle Materials," *Journal of Manufacturing Science and Engineering*, **137**(2015)1-8.
- [5] Rahman M.A., Rahman M., Kumar A.S., "Modelling of Flow Stress by Correlating the Material Grain Size and Chip Thickness in Ultra-Precision Machining," *International Journal of Machine Tools and Manufacture*, **123** (2017) 57–75.
- [6] Pan Z., Feng Y., Liang S.Y., "Material Microstructure Affected Machining: A Review" *Manufacturing Review*, **4** (2017) 1-12.
- [7] Vogler M.P., Kapoor S.G., Devor R.E., "On the Modeling and Analysis of Machining Performance in Micro-Endmilling, Part II: Cutting Force Prediction," *Journal of Manufacturing Science and Engineering*, **126**(2004), 695-705.
- [8] Lu X., Jia Z., Lu Y., Feng Y., Liang S. Y., "Predicting the Surface Hardness of Micro Milled Nickel-Base Superalloy Inconel 718," *International Journal of Advanced Manufacturing Technology*, DOI 10.1007/s00170-017-0512-x, 2017.
- [9] Kang I.S., Kim J.S., Kim J.H., Kang M.C., Seo Y.W., "A Mechanistic Model of Cutting Force in Micro End Milling Process," *International Journal of Material Processing Technology*, **187-188**(2007) 250-255.
- [10] Blanckenhagen, B. V., Gumbsh, P., Artz, E., "Dislocation Sources in Discrete Dislocation Simulations of Thin-Film Plasticity and the Hall-Petch Relation," *Modelling and Simulation in Materials Science and Engineering*, **9** (2001) 157–169.
- [11] Fernando B. O., Alessandro R. R., Reginaldo T. C., Adriano F. S., "Size Effect and Minimum Chip

- Thickness in Micromilling,"*International journal of Advanced Manufacturing Technology*, **89** (2015) 39-54.
- [12] Aramcharoen A., Mativenga P.T., (2009) "Size Effect and Tool Geometry in Micromilling of Tool Steel," *Precision Engineering*,**33**(2009) 402-407.
- [13] Arcona C., Dow T. A., (1998) "An Empirical Tool Force Model for Precision Machining,"*Transactions of the ASME*,**120** (1998) 700-707.
- [14] Fisk M., Ion J. C., Lindgren L. E., "Flow Stress Model for IN718 Accounting for Evolution of Strengthening Precipitates during Thermal Treatment,"*Computational Materials Science*,**82**(2014) 531-539.